# Optimal integration-based adaptive direction filter for InSAR interferogram

**YIN Hong-jie[1], LI Zhi-wei[1], DING Xiao-li[2], JIANG Mi[1], SUN Qian[1], WANG Ping[1]**

1. *School of Info-Physics and Geomatics Engineering, Central South University, Hunan, Changsha* 410083, *China*;
*2. Dept. of Land Surveying & Geo-Informatics, Hong Kong Polytechnic University, Hong Kong, China*

**Abstract:** In this paper, we present a new InSAR phase filtering method based on optimal integration. The algorithms can preserve very well the phase details while at the same time smoothing out the noise. Firstly, we use statistical method to determine the number of windows used for the filtering. It is an empirical constant associated with coherence. Secondly, eight linear directional windows are singled out, within each window a filtering is performed, and at the same time the mean coherence for each window is calculated. The proposed filtering will linearly combine a certain number (which has been determined in the first step) of the eight directional windows. However, directional windows with smaller filtering standard deviation will be given priority. Finally, the new phase value is calculated in terms of the weighted mean value of chosen linear windows. In this step, optimal integration is used to determine the weight of each directional window. The proposed filter is adaptively implemented by altering the number of the linear windows selected for filtering according to the coherence. Strategy of using both linear windows and optimal integration makes great difference in the filtering and achieve a good tradeoff between phase noise suppressing and signal preserving. Experimental results with both simulated and real data sets show that the new filter reduces the noise effectively while still minimizing the loss of signals.

**Key words:** optimal integration, direction smoothing, InSAR Interferogram, edge preservation, adaptive filter
**CLC number:** TP722.6/TP751.1 **Document code:** A

## 1 INTRODUCTION

Interferometric synthetic aperture radar (InSAR) has been successfully applied to measure surface topography (Zisk, 1972; Zebker & Goldstein, 1986) and monitor ground deformation (Massonnet *et al*., 1993; Ding *et al*., 2004) over time. However, the accuracy of the topography and deformation measurement is highly dependent on the quality of the interferogram (Li *et al.*, 2004). The application of InSAR to digital elevation model (DEM) production and deformation monitoring encounters problems due to noise in the interferometric phases, which is caused by various decorrelation factors, such as temporal, geometrical, Doppler centroid decorrelation, and thermal noise (Zebker & Villasenor, 1992). In addition to introducing noise into the DEM and deformation measurements, phase noise can also cause pseudo phase residues and hinder the process of phase unwrapping (Zebker & Villasenor, 1992).

Several techniques have been proposed in the literature to reduce interferometric phase noise. They mainly contains periodic mean filter (Eichel & Ghiglia, 1993), Goldstein spectrum filter (Goldstein & Werner, 1998; Baran *et al*., 2003; Li *et al*., 2008), adaptive complex filter (Lee *et al*., 1998), etc. The most commonly used filter by ESA and JPL is the boxcar mean filter applied in the complex plane, which usually blur the fringes of the interferogram. The adaptive filter proposed by Goldstein and Werner (1998) is implemented in the frequency domain and has been widely used in SAR data processing. It is easily used and can give very good result when the noise is not strong. However, when the noise is very strong, the filter does not work well, as most of the signals in the interferogram, especially the fringes and the edges will be filter out when using a large filter parameter $\alpha$ ($\alpha$ varies between zero and one). These errors will propagate into DEM and deformation measurements. The adaptive complex filter proposed by Lee *et al*. (1998) can preserve the edges effectively, as the filter conducts local phase unwrapping, gradient calculation, fringe detection, and directional window selection. These processes help a great deal in preserving fringes and edges, but on the other hand let the algorithm rather time-consuming. Moreover, the interferometric noise can cause errors in the step of phase unwrapping, which make the algorithm not robust. In this paper, we present the optimal integration and linear directional filter algorithms to the complex plane filter. The number of the linear windows used is deter-

**Received**: 2008-08-22; **Accepted**: 2008-11-18
**Foundation**: National Natural Science Foundation of China (No. 40774003, 40404001), National High-Tech. "863" Program of China (No. 2006AA12Z156), the Project of Western China 1:50000 Topography Mapping, the Project of Mineral Resources Conservation, Rational Exploitation of Hunan Lands Department, and Central South University Innovation Foundation for Postgraduate (No.2009ssxt173, 1343-74334000023).

**First author biography**: YIN Hong-jie (1983— ), male. His research interests include InSAR filtering and Digital image processing. E-mail: hongjieyin@126.com

mined according to the coherence of the interferogram.

This paper first introduces the directional filter algorithms of radar interferogram. Then the optimal integration-based adaptive direction filter algorithm will be discussed in details. In Section 4 and 5, the proposed filter will be validated with simulated and real data sets, respectively, followed by the conclusion.

## 2 DIRECTIONAL FILTER ALGORITHM

### 2.1 Phase noise characteristics

It has been validated that the phase noise in interferogram is additive and with zero mean (Lee *et al*., 1998). In the fringe-normal direction, the frequencies are in a wide band in which the real fringe signal and phase noise overlap and cannot be separated clearly. In contrast, in the fringe-tangential direction, the gray-level distribution is nearly constrained in a narrow band around zero, thus the fringe frequencies can be clearly separated from high-frequency noise. Consequently, on the fringe-tangential direction, a common low-pass filter, such as the mean or the median filter, can easily filter out the high-frequency noise without distortion of the real fringe signal (Yu *et al*., 2002).

Therefore, when the phase gradient is small, i.e., the phase changes slowly, we can do two-dimensional (2D) FFT and smooth the Fourier spectrum in frequency domain. In most cases, we can obtain satisfactory result. However, if the local topography or the deformation change vastly, the generated interferometric phase will include dense fringes and edges and also belong to high frequency components, which overlaps with noise and cannot be separated clearly. In this case, if filtering with directional window, we can easily filter out high-frequency noise without distortion of the real fringe and edge signal.

### 2.2 Directional filter algorithm (Yu *et al*., 2002)

Directional filter is also called spin filter in some literatures (e.g., Yu *et al*., 2002). Based on the noise characteristics (i.e., the gray-level changes slowly in the fringe-tangential direction), the filter conducts mean filter or median filter in directional window with small gray-level gradient. It can be implemented as the following steps:

(1) A window of $n\times n$ (e.g. 7×7) pixels is chosen. Within the window, eight isogonic lines in different directions are extracted as filtering lines. Fig. 1 shows the schemes of the isogonic lines.

(2) The mean and variance are calculated along each filtering line, and the one with the smallest variance is defined as fringe-tangential direction.

(3) Since the fringe-tangential direction is determined, one dimensional mean filter or median filter is implemented along that direction.

(4) A directional filter is completed by repeating the above process for every pixel over the whole image.

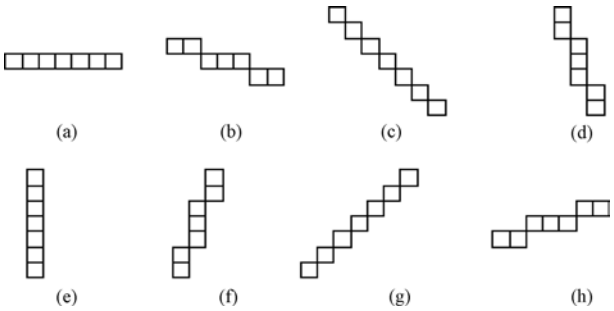


Fig. 1 Diagram of the direction of stripes

Directional filter first analyses the phase gradient by means of variance values, and then determine the filter line (i.e., the fringe-tangential direction) according to phase gradient, and finally implement the mean filter along the filter line. The algorithm minimizes signal loss of the interferogram especially the fringes and edges, when filtering out noise. But if the noise is strong, an interferogram is often under-filtered, as only 7 to 9 pixels are averaged in the filtering. If the interferogram is with low coherence and strong noise in large patch, the problem will become serious. Meanwhile, the edges in interferogram are often badly sharpened after applying the filtering, which also results in serious phase distortions.

## 3 OPTIMAL INTEGRATION-BASED ADAPTIVE DIRECTION FILTER

### 3.1 Line of thought

In Wavelet Transform-based image filtering, the image is decomposed into time-frequency domain, and then filtering is applied in each frequency. The filtered image can be reconstructed using the filtered frequency components. In this paper, we decompose the image into linear windows in several directions, and then optimal integration is adopted to rebuild the image using the filtered results in linear windows. As small variance criterion is used when selecting linear windows, i.e., the pixel with the smallest gradient is selected for filtering, which can greatly help to preserve the fringes and edges of the interferogram.

As we all know, the phase of an interferogram is wrapped, and the complex plane filter is used to solve the problem (Liao *et al*., 2003). The complex plane algorithm filters the real and the imaginary part of an interferogram respectively. Firstly, the mean value and variance of each linear directional window is calculated. Then a certain number (which has been determined use statistical method) of the eight directional windows are singled out and within each window a filtering is performed. Directional windows with smaller standard deviation (SD) will be given priority. Finally, the new phase value is calculated in terms of the weighted mean value of chosen linear windows. In

this step, optimal integration is used to determine the weight of each directional window. The new filtered phase image can be rebuilt using the filtered real and imaginary part of the interferogram.

### 3.2 Linear windows selection

To preserve the fringes and the edges, the filter window is particularly divided into eight linear windows. Fig. 1 shows the schemes of the eight linear windows. The approach can assure that the pixel selected for filtering is most similar to the true phase and can preserve the fringes and edges effectively.

The coherence between the two SAR images can be recognized as a direct measure of the interferometric phase noise. When the coherence is high, the phase noise appears low. On the contrary the noise is very strong when the coherence is low. In this paper, we relate the number of the filter windows chosen for filtering to the coherence. In areas of high coherence (less noise), we use less linear windows for filtering, which can assure that the phase will not be over-filtered. However, in the areas of low coherence (high noise), we use more linear windows for filtering, which can suppress the noise more effectively.

To determine the optimal number of linear windows used for filtering, we used the statistical method introduced by Li *et al*. (2008). Firstly, 500 DEMs are simulated with the universal multifractal technique. Then the phases of interferogram are simulated based on each of the simulated DEMs. In the process perpendicular baselines are chosen randomly between 50 and 200 m. The final phases are achieved by adding the interferometric noise simulated according to the coherence value. Finally, phase filtering is applied to the 500 simulated interferograms. For each interferogram, one to eight linear widows integration filtering are implemented separately. The RMS values calculated with the real phases as reference are used as criteria when evaluating the results. The result with the smallest RMS will be considered as optimal, and the number of linear widows for the optimal filtering is recorded. The results based on the simulated studies are given in Table 1.

**Table 1 Statistics of results for determining the optimal number of liner windows for different coherence**

| Coherence | Number of occurrences of linear windows 1, 2, …, 8 as optimal value | | | | | | | |
|---|---|---|---|---|---|---|---|---|
| | 1 | 2 | 3 | 4 | 5 | 6 | 7 | 8 |
| 0.1 | 0 | 0 | 0 | 0 | 0 | 0 | 0 | 500 |
| 0.2 | 0 | 0 | 0 | 0 | 0 | 0 | 0 | 500 |
| 0.3 | 0 | 0 | 0 | 3 | 23 | 43 | 48 | 383 |
| 0.4 | 3 | 1 | 47 | 1 | 10 | 254 | 142 | 42 |
| 0.5 | 43 | 246 | 67 | 35 | 17 | 12 | 7 | 73 |
| 0.6 | 338 | 134 | 12 | 1 | 0 | 0 | 4 | 11 |
| 0.7 | 367 | 118 | 9 | 1 | 1 | 0 | 1 | 3 |
| 0.8 | 314 | 140 | 21 | 2 | 2 | 4 | 9 | 8 |

According to the statistic results based on totally 32000 times filtering of the simulated interferograms, as shown in Table 1, we can get the optimal empirical constant of the number of linear windows chosen for filtering with different coherences:

$$N=\begin{cases}0 & \text{when } \gamma>0.8\\ 1 & \text{when } 0.5<\gamma\leqslant 0.8\\ 2 & \text{when } 0.4<\gamma\leqslant 0.5\\ 6 & \text{when } 0.3<\gamma\leqslant 0.4\\ 8 & \text{when } \gamma\leqslant 0.3\end{cases} \tag{1}$$

where $\gamma$ is coherence value, and $N$ is the number of the linear widows. when $N$=0, no filtering will be done.

### 3.3 Optimal integration (Gong *et al*., 2007; Li *et al*., 1998)

The new phase value is calculated in terms of the weighted mean value of chosen linear windows. Optimal integration is used to determine the weight of each directional window. In this study, the weight is determined based on the reciprocal of standard deviation. The optimal integration-based adaptive direction filter can then be written as:

$$\hat{m}=\sum_{i=1}^{N} w_i m_i \tag{2}$$

where $\hat{m}$ is the filtered value, $m_i$ and $w_i$ is the mean and the corresponding weight of the $i^{\text{th}}$ linear window, and $N$ is the number of the linear windows used for filtering. In Eq.(2) the weight $w_i$ is calculated as follows:

$$w_i=\frac{1/\sigma_i^2}{\sum_{K=1}^{N}1/\sigma_k^2}\quad i=1,2,\cdots,N \tag{3}$$

where $\sigma_i^2$ is the variance of $i^{\text{th}}$ linear window. Following the statistic theory, we can get that the variance of the filtering value is less than that of any selected linear window:

$$\bar{\sigma}^2=\frac{1}{\sum_{k=1}^{N}\frac{1}{\sigma_k^2}}<\min\left(\sigma_i^2,i=1,2\cdots N\right) \tag{4}$$

So the proposed filtering has better noise reduction than that of

any single linear window.

### 3.4 Algorithm description

The developed optimal integration-based adaptive direction filter can be implemented following the steps of:

(1) Filter the phase image by a 3×3 complex mean boxcar filter. This is a preparatory step that intents to improve the robustness of variance estimation.

(2) Compute the phase standard deviation and mean value of the eight linear directional windows. The sketch map is shown in Fig. 1.

(3) Select the number of linear directional window $N$ used for filtering according to the coherence value. The relationship of the number of directional windows and coherence value is shown in Eq.(1). In the linear filter windows selection, directional windows with smaller filtering standard deviation will be given priority. Meanwhile the weights will be calculated by Eq.(3).

(4) Combine the selected directional windows using optimal integration method. In this step, the mean value of the $N$ directional widow is linearly combined with the weights calculated based on the reciprocal of standard deviation.

In addition, we have taken two measures to improve the robustness of the algorithm. Firstly, the center pixel is not included in the calculation of the mean and variance of the directional windows, which make great sense when the pixel is noise itself. Secondly, the introduction of the 3×3 preparatory mean boxcar filter, which can improve the accuracy of the variance evaluation and thus the optimal integration accuracy.

In optimal integration, the weight of the directional window is determined based on the reciprocal of the standard deviation, which makes the weight of the pixel wiht small gradient large. So the filter can preserve the fringes and the edges of the phase perfectly, while at the same time suppress the noise effectively. In the study, we find that using linear windows of less than four can almost make no distortion to the fringes and the edges. Experiments of filtering the noise-free interferogram show that the edge preservation index is larger than 0.9 and the RMS keeps smaller than 0.1. So the directional filtering with less linear windows can be used iteratively where the noise is strong.

## 4 VALIDATION WITH SIMULATED DATA

The performance of the new filter will be evaluated with simulated data set in this section. The noise-free interferogram is simulated by GAMMA software using the true DEM of Lengshuijiang County, Hunan province, with the parameters of L band and perpendicular baseline of 258 m. A coherence map is also simulated considering the thermal, the temporal and the geometrical decorrelation (Hanssen, 2001). A phase SD table is obtained based on the coherence map. Then the phase noise are simulated based on the corresponding phase SD table and added to the noise-free interferogram to form the experiment interferogram (Baran *et al*., 2003). The performance of the new filter is evaluated by comparing the filtered interferogram with the original noise-free one.

To validate the performance of the new filter, comparisons with Lee filter (Lee *et al*., 1998) and Goldstein filter (the parameter $\alpha$ is adopted as 0.5) (Goldstein & Werner, 1998) will be made. The simulated interferogram and the interferograms filtered with the above three filters are shown in Fig. 2.

Fig. 2 shows that the new filter has the strengths of both the Goldstein and the Lee filters. It can not only filter out noise like Goldstein filter, but also preserve the fringes and edges as Lee filter. The filter can minimize the signal loss while at the same time suppress phase noise effectively. For a closer examination of the results, cross sections of line 250 are extracted from each of the filtered interferogram and the original phase. The diagram of the cross sections is shown in Fig. 3. It is obvious that the phase by the new filter is smooth and with sufficient details. Comparing the results of the three filters with the original phase, we can see the results of the new filter have nearly the same profiles as that of the original noise-free interferogram. The new filter preserves the signal details perfectly, and is of great fidelity to the original phase.

For a quantitative evaluation of the performance of the filters, the following assessment criteria are adopted:

(1) Phase standard deviation (PSD). The criterion is a measure of the phase smoothness, and the smaller the PSD, the smoother the phase. It is calculated as follows (Goldstein & Werner, 1998):

$$\mathrm{PSD}=\sum\left(\frac{\sum_N(\phi(i,j)-\bar{\phi}(i,j))^2}{N-1}\right)^{\frac{1}{2}} \tag{5}$$

where $N$ is the number of samples in the window, $\phi(i,j)$ is the phase of the pixels in the window, $\bar{\phi}(i,j)$ is the complex mean value of the pixels in the window, and $i$ is the line number and $j$ is the width number.

(2) Edge Preservation Index (EPI). The criterion is a measure of the capability of fringe and edge preservation. The closer the value to 1, the better the fringe and edge preservation in the filtered interferogram. It is calculated as follows (Han *et al*., 2003):

$$\mathrm{EPI}=\frac{\sum\left(\left|\phi_{\mathrm{s}}(i,j)-\phi_{\mathrm{s}}(i+1,j)\right|+\left|\phi_{\mathrm{s}}(i,j)-\phi_{\mathrm{s}}(i,j+1)\right|\right)}{\sum\left(\left|\phi_0(i,j)-\phi_0(i+1,j)\right|+\left|\phi_0(i,j)-\phi_0(i,j+1)\right|\right)} \tag{6}$$

where $\phi_{\mathrm{s}}(i,j)$ is the filtered phase and $\phi_0(i,j)$ is the reference phase. However, as the phase of the interferogram is wrapped, the difference of the original and filtered phases can be close to $2\pi$, rather than a small value. In this case, the phases are actually approximately the same, and the error is caused by the phase wrapping. To minimize the effect of phase wrapping,

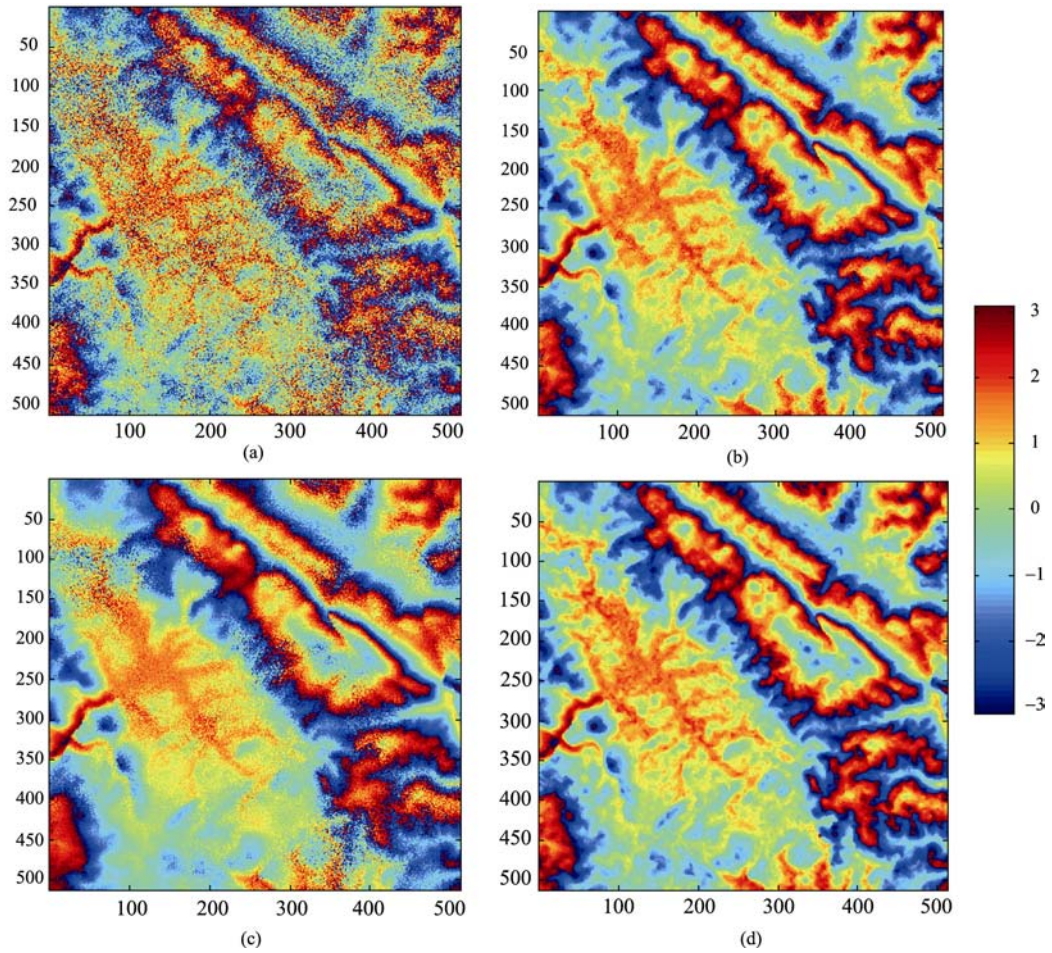


Fig. 2 Simulated interferogram and their filtered versions with three filters
(a) Simulated phase with noise; (b) Results of Lee filter; (c) Results of Goldstein filter; (d) Results of New filter

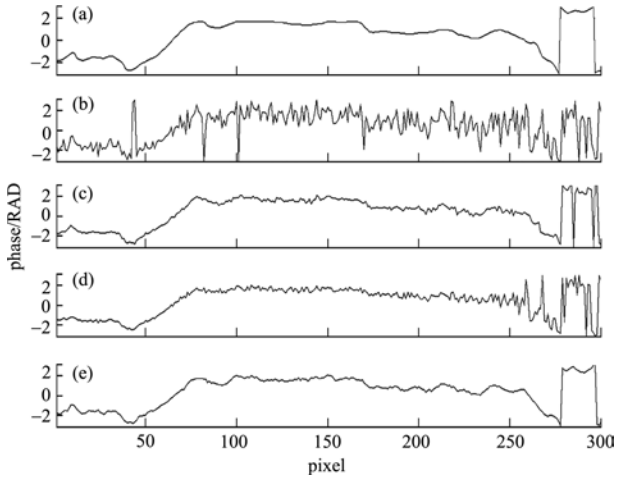


Fig. 3 Cross sections of line 250 of the simulated and the filtered interferograms
(a) Original Phase; (b) Phase with Noise; (c) Lee Filter; (d) Goldstein Filter; (e) New Filter

we calculate the difference of the two pixels by adding or subtracting 2π in this paper. The same strategy is also used in the following RMS calculation.

(3) Root Mean Squares (RMS). The criterion measures the deviation of the filtered interferogram to the reference one, i.e., the simulated noise-free interferogram. The smaller the RMS, the closer the filtered phases to reference phases. It is calculated as follows:

$$\mathrm{RMS}=\sqrt{\frac{\sum\left(\phi_{\mathrm{s}}(i,j)-\phi_0(i,j)\right)^2}{N-1}} \tag{7}$$

where $\phi_{\mathrm{s}}(i,j)$ is the filtered phase, and $\phi_0(i,j)$ is the reference phase. $N$ is the number of samples in the window.

(4) Phase residues (Liao & Lin, 2003). Residues mean phase inconsistency or jump in the interferogram. They are caused by phase noise or natural topographic jump. The less the residues, the better the quality of an interferogram. Thus, it is one of the most important and widely used criteria for filters evaluation.

**Table 2 Evaluation results of different filters**
(simulated interferogram)

| Filter algorithm | PSD | EPI | Phase residue | RMS/rad |
|---|---|---|---|---|
| Noise-free interferogram | 92762 | – | – | – |
| Noisy interferogram | 324490 | 8.5053 | 16287 | 0.9142 |
| Lee Filter | 116380 | 1.6473 | 2 | 0.2381 |
| Goldstein Filter | 157520 | 3.4335 | 1313 | 0.4416 |
| New Filter | 101310 | 1.0595 | 4 | 0.2015 |

The numerical validation results of the filters are listed in Table 2. Contrast to Goldstein filter and Lee filter, the new filter has smaller PSD and RMS values, indicating the interferogram filtered by the new filter is smoother. A further study shows that the PSD of the new filter is smaller than that of Goldstein filter when adopting filtering parameter $\alpha$=0.9. Moreover, the EPI of the new filter is closer to 1 than the Goldstein and the Lee filter, *i.e.*, the new filter preserves better the fringe and edge. Therefore, the new filter has not only better smooth capability, but also better signal details preservation. As for residues reduction, the new filter is almost the same as Lee filter, with a reduction rate of 99.98%. The new filter show strong ability in residues reduction.

## 5 VALIDATION WITH REAL DATA

An ALOS PALSAR pair acquired on 19 June and 19 September 2007 over Henan province will be used to assess the performance of the new filter. The perpendicular baseline and the temporal baseline are about 282m and 90 days respectively. The SAR images are processed with GAMMA software until an interferogram with curved Earth phase trend removed is got. We choose a region of $1000\times1000$ pixels with significant topography so that there are plenty of fringes and edges in the interferogram. The interferogram is filtered with the new, the Goldstein and the Lee filters and the results are shown in Fig. 4.

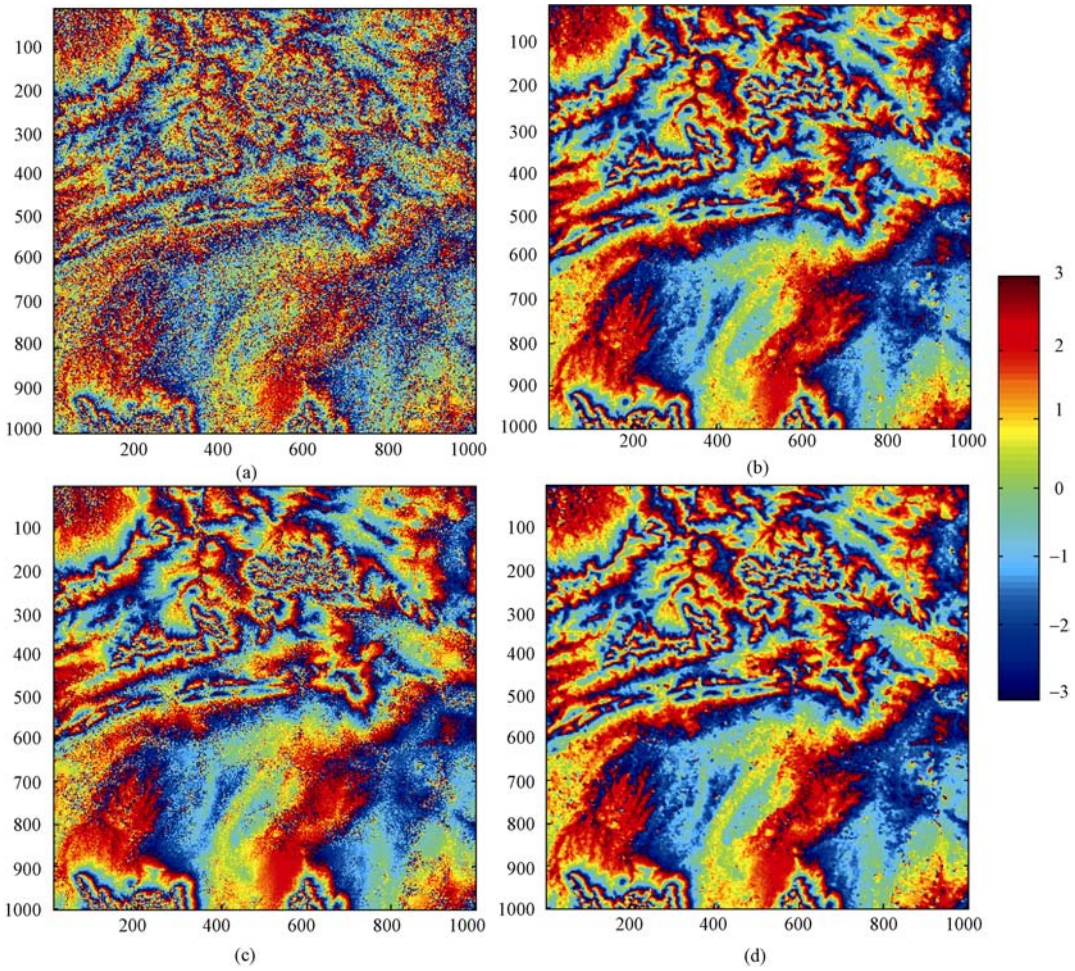


Fig. 4 Real interferogram filtered with 3 filters

(a) Original phase; (b) Results of Lee Filter; (c) Results of Goldstein Filter; (d) Results of New Filter

The results show that the new filter can filter out the noise effectively while at the same time preserve the details of the interferogram. Especially in the upper-middle part of the interferogram, the phase is reconstructed very well by the new filter. However, the results of Goldstein filter appear rather blurring. The numerical statistic results are shown in Table 3. From Table 3, we can see easily the new filter performs much better than the Goldstein and the Lee filter in both the criteria of PSD and phase residues. Most importantly, with the need of phase unwrapping, the Lee filter is rather time-consuming. In this experiment, Lee filter costs almost six hours (Table 3).

## 6 CONCLUSIONS

The proposed filter is adaptively implemented by altering the number of the linear windows selected for filtering. Coherence is chosen as parameter to determine the number of the linear filtering windows. Optimal integration is used to

**Table 3 Evaluation results of different filters**
(real interferogram)

| Filter Algorithm | PSD | Phase residues | Reduction Rate of phase residues/% | Operating Time/min |
|---|---|---|---|---|
| Real Interferogram | 1507300 | 137177 | – | – |
| Lee Filter | 641210 | 1412 | 98.97 | 349.75 |
| Goldstein Filter | 972610 | 29009 | 78.85 | 1.32 |
| New Filter | 514330 | 939 | 99.31 | 6.18 |

combine the selected directional windows. The linear directional windows, which are selected based on the fringe frequencies characteristic of tangential direction, make great sense in fringe preservation. The new filter considers the local statistic characteristic of the interferogram and can be implemented adaptively by the introduction of coherence. In the areas of low coherence (high noise), more linear windows are included for filtering, which can suppress noise more effectively. However, in areas of high coherence (less noise), less linear windows are used for filtering which can assure that the phase is not over-filtered. Experimental results with both simulated and real data sets of L-band show that the filter proposed in this paper can filter out noise efficiently and have almost no blurring effect and phase distortion to the interferometric fringes.

In this study, we find that signal loss cannot be avoided because of the intrinsic restriction of filtering, whatever we modify the filter to. Especially, when the noise is strong (the coherence is smaller than 0.1), most filters cannot give satisfied result. When the noise component is more than that of the signal, the phase can not be reconstructed by filtering.

The proposed algorithm performs very well in phase noise suppressing and signal details preserving. However, when the fringe is quite dense, the result is not promising. In addition, the complication of the algorithm is yet to be improved and further study are still needed in the future.

**Acknowledgements:** The images used in the paper are provided by Japan Aerospace Exploration Agency under project AO-430.

## REFERENCES

Baran I, Stewart M P, Kampes B M, Perski Z and Lilly P. 2003. A modification to the Goldstein radar interferogram filter. *IEEE Trans. Geosci. Remote Sensing*, **41**(9): 2114—2118

Ding X L, Liu G X, Li Z W, Li Z L and Chen Y Q. 2004. Ground subsidence monitoring in Hong Kong with satellite SAR interferometry. *Photogrammetric Engineering and Remote Sensing*, **70**(10): 1151—1156

Eichel P H and Ghiglia D C. 1993. Spotlight SAR Interferometry for Terrain Elevation Mapping and Interferometric Change Detection. Sandia National Labs. Tech. Report

Goldstein R M and Werner C L. 1998. Radar interferogram filtering for geophysical applications. *Geophy. Res. Lett*., **25**(21): 4035—4038

Gong C L. 2007. Image smoothing method based on data fusion technology. *Journal of Jiaying University* (*Natural Science*), **25**(3): 81—84

Han C M, Guo H D, Wang C L , Fan D and Sang H Y. 2003. Edge-preserving filter for SAR images. *Chinese High Technology Letters*, **7**: 11—15

Hanssen R H. 2001. Radar Interferometry: Data Interpretation and Error Analysis. Kluwer Academic Publishers Netherlands

Lee J S, Papathanassiou K P, Ainsworth T L, Grunes M R and Reigber A. 1998. A new technique for noise filtering of SAR interferogram phase images. *IEEE Trans. Geosci. Remote Sensing*, **36**(5): 1456—1465

Li Z L, Zou W B, Ding X L, Chen Y Q and Liu G X. 2004. A quantitative measure for the quality of InSAR interferograms based on phase differences. *Photogrammetric Engineering and Remote Sensing*, **70**(10): 1131—1137

Li Z W, Ding X L, Huang C, Zhu J J and Chen Y L. 2008. Improved filtering parameter determination for the goldstein radar interferogram filter. *ISPRS Journal of Photogrammetry and Remote Sensing*, **63**: 621—634

Li Z Y, Li G D and Zhang J X. 1998. Multi-sensor data fusion and Simulation. *Journal of Jiangsu University* (*Natural Science Edition*), **19**(6): 95—100

Liao M S and Lin H. 2003. Synthetic Aperture Radar Interferometry: Principle and Signal Processing. Beijing: Mapping Press

Liao M S, Lin H , Zhang Z X, Yang W and Zhang L. 2003. Adaptive algorithm for filtering interferometric phase noise. *Journal of Remote Sensing*, **7**(2): 98—105

Massonnet D, Rossi M, Cesar C, Frederic A, Gilles P, Kurt F and Thierry R. 1993. The displacement field of the Landers earthquake mapped by radar interferometry. Nature, **364**(8): 138—142

Yu Q F, Lu H W and Liu X L. 2002. Image-based Precise Measurement and Movement Measurement. Beijing: Science Press

Zebker H A and Goldstein R M. 1986. Topographic mapping from interferometric synthetic aperture radar observations. *J. Geophy. Res*., **91**(BS): 4993—4999

Zebker H A and Villasenor J. 1992. Decorrelation in interferometric radar echoes. *IEEE Trans. Geosci. Remote Sensing*, **30**(5): 950—959

Zisk S H. 1972. A new Earth-based radar technique for the measurement of lunar topography. *Moon*, **4**: 296—306

# InSAR 干涉图最优化方向融合滤波

尹宏杰[1], 李志伟[1], 丁晓利[2], 蒋 弥[1], 孙 倩[1], 王 平[1]

1. 中南大学 测绘与国土信息工程系, 湖南 长沙 410083;
2. 香港理工大学 土地测量与地理资讯学系, 香港 九龙

摘 要: 在分析干涉条纹图噪声特征的基础上, 提出了一种能有效保持干涉图条纹的边缘和细节信息的 InSAR 干涉图滤波算法——基于最优化融合的自适应方向平滑算法。该算法首先对 8 个线性方向窗口进行统计分析, 然后根据干涉图的相干性选择合适的线性方向窗口, 按照最优化融合的方法, 以方差倒数为权重对各个方向窗口的均值进行加权平均。模拟和真实干涉图数据的实验结果表明新方法不仅能有效的抑制干涉图噪声, 而且能较好的保持干涉图的细节和边缘信息, 具有很好的信息保持能力。

关键词: 最优化融合, 方向平滑, InSAR 干涉图, 边缘保持, 自适应滤波

中图分类号: TP722.6/TP751.1 文献标识码: A

## 1 引 言

合成孔径干涉雷达(InSAR)以其高分辨率和高精度的特点, 被广泛应用于地形测量(Zisk, 1972; Zebker & Goldstein, 1986)和地表形变的监测(Massonnet 等, 1993; Ding 等, 2004)。然而, DEM 和地表形变监测的精度在很大程度上取决于干涉图的质量(Li 等, 2004)。目前, 时间失相关、几何失相关、多普勒中心频率失相关和热噪声等失相关噪声是制约 InSAR 技术精度的重要因素(Zebker & Villasenor, 1992)。干涉失相关可以引起干涉图的强噪声, 直接影响干涉生成的数字高程模型的精度。此外, 干涉失相关噪声还能引起干涉相位的奇异点(相位突变点), 阻碍干涉相位解缠等(Zebker & Villasenor, 1992)。

针对干涉图失相关噪声, 提出了一些滤波算法。主要包括: 圆周期均值法(Eichel & Ghiglia, 1993), Goldstein 的谱平滑法及其改进算法(Goldstein & Werner, 1998; Baran 等, 2003; Li 等, 2008), 局部坡度自适应滤波法(Lee 等, 1998)等。均值法是目前欧洲空间局和 JPL 广泛使用的方法, 然而它容易使干涉条纹边缘变得模糊。Goldstein 等(1998)的谱平滑法是目前广泛使用的一种方法, 它使用简单, 而且在噪声不强的情况下滤波效果很好。在强噪声情况下, Goldstein 的谱平滑法滤波效果并不能令人满意, 因为采用高滤波因子进行滤波时, 在去除噪声的同时, 会带走大量干涉图的信息, 尤其是边缘信息, 为 DEM 和形变测量引入误差。Lee 等(1998)提出的局部坡度自适应滤波法在实际中由于要求坡度值、检测条纹边缘的位置和判断边缘的方向, 又要引入复杂的相位解缠, 使其变得复杂、耗时, 可操作性不强。而且由于干涉图的噪声影响, 会给相位解缠带来误差, 算法的稳健性有待改善。

针对 Lee 滤波的缺点, 本文将最优化融合方法引入干涉图复数图像滤波, 结合方向平滑算法, 根据干涉图的相干性选择融合方向窗口的数量。

## 2 干涉图方向平滑算法

### 2.1 干涉图条纹及其噪声的分布规律

干涉相位图中的噪声是统计特性为零均值的加性噪声(Lee 等, 1998)。在条纹法线方向,灰度变化较大, 对应的频谱呈一条宽带, 条纹信号与噪声频谱

收稿日期: 2008-08-22; 修订日期: 2008-11-18

基金项目: 国家自然科学基金(编号: 40774003, 40404001); 国家 863 专题项目(编号: 2006AA12Z156); 国家西部 1:50000 空白区测图工程 2007 年度研究课题; 湖南省国土资源厅矿产资源保护与合理开发利用科研项目, 中南大学研究生教育创新工程(编号: 2009ssxt173, 1343-74334000023)。

第一作者简介: 尹宏杰(1983— ), 男, 河南商丘人, 中南大学摄影测量与遥感专业研究生, 主要从事 InSAR 干涉图滤波、InSAR 理论及应用技术研究。E-mail: hongjieyin@126.com。

叠加在一起，无法截然分开。在条纹切线方向，灰度变化很小，近似为常数，对应的频谱为零频附近的一条窄带，随机噪声仍然分布在高频段，使用常规的低通滤波器，如中值滤波或均值滤波，就可将零频条纹与高频噪声频谱干净地分离开，从而可以达到既滤掉噪声又不对条纹产生模糊畸变效应的目的(于起峰等, 2002)。

因此，在相位变化不快，相位梯度较小的区域，通过傅立叶变换把相位转化到频域对频谱进行修剪去除高频成分，可以有效的去除噪声，取得很好的平滑效果。值得注意的是：当地形或形变复杂导致相位细节丰富时，条纹及边缘信号同样属于高频成分，与噪声频谱叠加在一起，无法截然分开。此时，选择方向窗口进行滤波，则可以在有效去除噪声的同时保留边缘和细节的信息。

### 2.2 方向平滑算法(于起峰等, 2002)

方向平滑算法也称旋滤波，该方法根据条纹图在切线方向灰度变化最小的特点，选择灰度变化最小的线性方向窗口对条纹图进行均值或中值滤波。其实现步骤为:

(1) 在以当前点为中心的 $n\times n$ 像元点的窗口内，定义 8 条(也可以取 16 或 32 条)等角度间隔的方向滤波线，图 1 为 8 个方向的示意图。

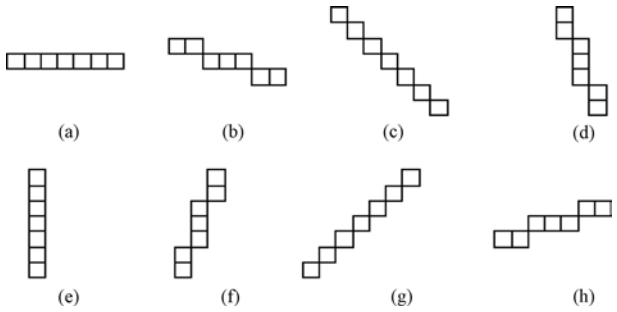


图 1 条纹方向示意图

(2) 计算每个方向线上各点灰度值的均方差，该值最小的方向线定义为条纹的切线方向。

(3) 当条纹的切线方向确定后，用一维中值滤波或均值滤波在该切线方向进行滤波。

(4) 对条纹图全场每个点重复上述过程。

方向平滑算法根据方差的大小分析坡度信息，根据坡度决定滤波窗口的方向，对所选滤波窗口的像元求取均值代替像元的原始数值。该算法最大程度的保留干涉条纹图细节尤其是边缘信息，具有较高的保真性。但是，该算法的平滑效果不佳，尤其是当噪声很强、相干性很低的区域，该方法的去噪效果很差。而且该方法采取同一梯度的线性窗口进行滤波，会引起边缘信息的强化，同样会造成干涉图条纹图失真。

## 3 基于最优化融合的自适应方向平滑算法

### 3.1 最优化融合方向平滑算法的基本思路

在小波分析图像处理中，通常采用频谱分解的方法，即在不同频率对图像进行分解平滑，然后进行重构。本文对空间域不同的方位方向以线性窗口的形式进行分解、平滑，然后按照最优化的方法进行图像的重构。由于线性窗口是选择方差最小的区域，该区域和原始像元具有非常相近的坡度，因而能够最大限度的保留干涉图的细节和边缘信息。

由于 InSAR 干涉条纹图存在固有的相位跳变，所以采用复数域滤波的方法(廖明生等, 2003)。把相位分解成正弦部分和余弦部分分别进行滤波，首先计算每个线状方向窗口的正余弦部分的均值及方差，然后根据所选区域的平均相干性确定需要选取的线性窗口的个数 $N$，最后用最优化融合方法对所选方差最小的 $N$ 个线性窗口的均值进行加权平均得到最终结果。根据滤波后正弦和余弦数据重构干涉相位图。

### 3.2 线状平滑窗口的选择

为了提高边缘保持能力，本文对滤波窗口进行细致划分，选择 8 个线性窗口，如图 1。这种方向掩模窗口可检测到在中心点处 8 个方向的线状均匀区域，从而保证选择与原始相位相似区域的像素滤波，最大程度的保留干涉图的边缘和细节信息。

由于干涉图的相干性和噪声强弱具有高相关性，相干性高的区域其干涉图噪声也较小，相干性低的区域其噪声则比较大。本文根据相干性的大小选择线性窗口的数量，在相干性高的区域其噪声较弱，此时采用较少的线性窗口进行融合滤波，减少信息损失；在相干性低的区域其噪声较强，选择较多线性窗口进行融合滤波，增强去噪能力。

为得到线性窗口个数的最优值，本文参照 Li 等(2008)获取参数的方法，对大量数据进行统计分析。首先，根据多分形理论生成 500 幅 DEM；然后，随机采用 50—200m 的垂直基线模拟 DEM 对应的干涉图，并根据不同相干系数对应的相位标准偏差添加噪声。最后，对 500 幅干涉图分别采用 1—8 个数目不同的线性窗口进行滤波，以不含噪声的干涉图作为参考计算 RMS 值，取 RMS 值最小的滤波为最优滤波，统计线性窗口个数 $N$ 分别为 1, 2, …, 8 时达到最优滤波的次数，统计结果见表 1。

**表 1** 不同相干系数下线性窗口个数 **N** 最优值统计表

| 相干系数 | 线性窗口个数 $N$ 分别为 1, 2, …, 8 时达到最优滤波的次数 | | | | | | | |
|---|---|---|---|---|---|---|---|---|
| | 1 | 2 | 3 | 4 | 5 | 6 | 7 | 8 |
| 0.1 | 0 | 0 | 0 | 0 | 0 | 0 | 0 | 500 |
| 0.2 | 0 | 0 | 0 | 0 | 0 | 0 | 0 | 500 |
| 0.3 | 0 | 0 | 0 | 3 | 23 | 43 | 48 | 383 |
| 0.4 | 3 | 1 | 47 | 1 | 10 | 254 | 142 | 42 |
| 0.5 | 43 | 246 | 67 | 35 | 17 | 12 | 7 | 73 |
| 0.6 | 338 | 134 | 12 | 1 | 0 | 0 | 4 | 11 |
| 0.7 | 367 | 118 | 9 | 1 | 1 | 0 | 1 | 3 |
| 0.8 | 314 | 140 | 21 | 2 | 2 | 4 | 9 | 8 |

根据表 1 对不同相干系数的 500 幅模拟干涉图的 32000 次滤波结果进行统计分析，可得不同相干系数下最优滤波窗口个数 $N$ 的经验取值，如式(1)

$$N=\begin{cases}0 & \gamma>0.8\\ 1 & 0.5<\gamma\leqslant 0.8\\ 2 & 0.4<\gamma\leqslant 0.5\\ 6 & 0.3<\gamma\leqslant 0.4\\ 8 & \gamma\leqslant 0.3\end{cases} \tag{1}$$

式中，$\gamma$ 为相干值，$N$ 为滤波窗口的个数，取 0 表示不对该像元进行滤波处理。

### 3.3 最优化融合方法(龚昌来等, 2007; 李智勇等, 1998)

对所选线性滤波窗口的均值以方差倒数为权重，求线性窗口的加权平均值来代替像元的值。其计算公式为

$$\hat{m}=\sum_{i=1}^{N}w_i m_i \tag{2}$$

式中，$\hat{m}$ 为融合估计值，$m_i$ 和 $w_i$ 分别为第 $i$ 个线性窗口的相位平均值和权值，$N$ 为所选线性窗口个数。权重 $w_i$ 计算公式为

$$w_i=\frac{1/{\sigma_i}^2}{\sum_{K=1}^{N}1/\sigma_k^2}\quad i=1,2,\cdots,N \tag{3}$$

式中，${\sigma_i}^2$ 为第 $i$ 个线性窗口的方差，$N$ 为所选线性窗口个数。由概率统计理论可求得融合估计值的方差为

$$\hat{\sigma}^2=\frac{1}{\sum_{k=1}^{N}\frac{1}{\sigma_k^2}}<\min\left(\sigma_i^2,i=1,2\cdots N\right) \tag{4}$$

由式(4)可知，融合估计值的方差比 $N$ 个线性窗口中最小的方差小。因此平滑效果要优于单个线性窗口的平滑效果。

### 3.4 最优化融合方向平滑算法的实现

(1) 用 3×3 的小窗口进行均值滤波，对干涉图进行预滤波。从而减少噪声对方差估计的影响，增强估计的稳健性。

(2) 在 7×7 的滤波窗口中，分别计算图 1 中 8 个线性方向窗口的方差和均值。

(3) 根据相干性按式(1)选择进行融合的线性窗口个数，根据方差大小对所有 8 个线性窗口进行降序排列，选择方差较小的 $N$ 个线性窗口，并按式(3)计算其权值。

(4) 按照最优化融合方法，以方差倒数为权对所选的 $N$ 个线性窗口的均值进行加权平均，计算像元值来代替原始值，实现对所选 $N$ 个线性窗口的最优化融合。

为了增强最优融合估计的鲁棒性和容错性，本文采用两个措施：一是中心像元 C 不参与均值和方差的运算，防止中心像元本身即为噪声点；二是采用 3×3 的滤波窗口进行均值预滤波，以降低噪声对求标准差的影响,然后再进行融合处理。

采用线性方向窗口融合的方法，由于采用方差倒数进行加权的方法，使得在相位相似的区域的权重变大。不仅很好的保持了干涉图边缘信息和细节，而且有很好的去噪效果。在本文研究中也发现，在选择 4 个以下线性窗口进行融合时能很好的保持原干涉图的信息，对不含噪声的干涉图实验表明边缘保持指数在 0.9 以上, RMS 在 0.1 rad 左右，不会影响地形测量和形变监测的精度。因此，在强噪区域可以采用较少的线性窗口进行二次迭代滤波，从而达到较好的滤波效果。

## 4 模拟数据的验证

为了检验方法的有效性，本文首先采用了模拟数据进行验证。模拟干涉图采用湖南省冷水江市锡矿山的真实 DEM，采用参数为 L 波段、垂直基线 258m，用 Gamma 软件获得该地区的模拟相位图。为

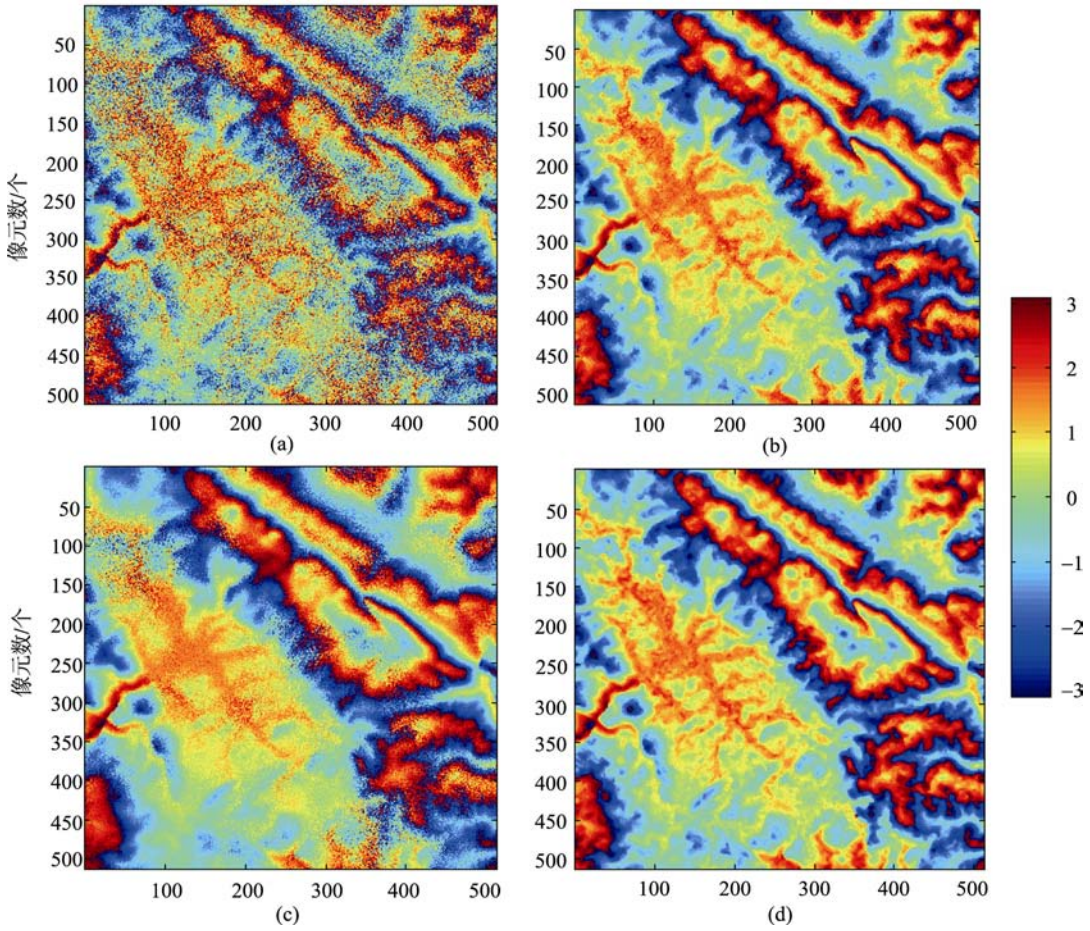


图 2　3 种滤波后的模拟干涉相位图

(a) 加噪模拟相位图; (b)Lee 滤波; (c) Goldstein 滤波; (d) 新方法滤波

实现自适应滤波，本文根据系统热噪声、时间失相关和空间失相干等失相干源，模拟了干涉图对应的相干性信息(Hanssen, 2001)。根据模拟相位的相干值，得到对应的相位标准偏差，对该地区的模拟相位数据进行加噪(Baran 等，2003)。通过与未加噪的模拟相位图进行对比验证，对新滤波方法进行评估。

本文算法同 Lee 滤波，以及频域经典的 Goldstein 滤波方法(采用滤波因子 0.5)进行比较。图 2 为加噪后的模拟干涉相位图和采用 3 种滤波方法滤波得到的干涉相位图。

从图 2 的滤波结果可看出本文算法不仅具有频域经典 Goldstein 滤波相位平滑的特点，而且保留了和 Lee 滤波相当的相位细节及边缘信息。新的滤波器在噪声抑制和信息保持上表现出了良好的特性。取相位图第 250 行数据作为剖面，图 3 为得到的剖面数据绘制的散点图。从图 3 可以看出本文采用的滤波方法相位平滑、细节丰富。对各滤波结果剖面进行对比分析，发现新方法滤波结果具有和未加噪的模拟数据几乎相同的剖面信息，较为完整的复原了原始干涉图的信息，具有很高的保真性。

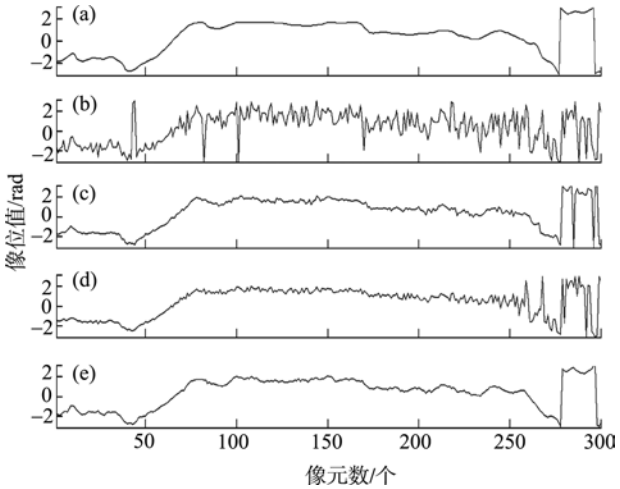


图 3　模拟干涉相位图滤波结果第 250 行剖面图

(a)原始相位; (b) 含噪相位; (c) Lee 滤波; (d) Goldstein 滤波; (e) 新滤波

为了定量的评价相位图的平滑效果和保真性，本文采用如下定量指标对干涉相位图进行评价:

(1) 相位标准偏差(PSD)(Goldstein & Werner, 1998)。该因子为反映相位的平滑度指标，其值越小

表示相位越平滑。计算公式为:

$$\mathrm{PSD}=\sum\left(\frac{\sum_N(\phi(i,j)-\bar{\phi}(i,j))^2}{N-1}\right)^{\frac{1}{2}} \tag{5}$$

式中，$\phi(i,j)$ 是干涉图相位值，$\bar{\phi}(i,j)$ 是所选滑动窗口干涉图相位值的平均值。$N$ 是滑动窗口像元个数，$i$ 是像元的行数，$j$ 是像元的列数。

(2) 边缘保持指数 EPI (Edge Preservation Index) (韩春明等, 2003)。该因子反映滤波结果的边缘信息的保持能力，该指标越接近于 1，表示滤波后的相位图和参考相位图在梯度及边缘信息上越接近。计算公式为:

$$\mathrm{EPI}=\frac{\sum\left(\left|\phi_s(i,j)-\phi_s(i+1,j)\right|+\left|\phi_s(i,j)-\phi_s(i,j+1)\right|\right)}{\sum\left(\left|\phi_0(i,j)-\phi_0(i+1,j)\right|+\left|\phi_0(i,j)-\phi_0(i,j+1)\right|\right)} \tag{6}$$

式中，$\phi_s(i,j)$ 是滤波后的相位值，$\phi_0(i,j)$ 是参考干涉图相位值。由于 2π相位跳变不会引起相位解缠的误差，因此，实际的计算中，在相位跳变点我们采用加减 2π的方法来消除因相位跳变产生的计算误差。均方误差计算中，我们采用了同样的方法。

(3) 均方误差(RMS)。该因子以未加噪的相位图作为参考值，计算滤波后相位图和参考相位图产生的偏差，其值越小代表滤波器的保真性越好。计算公式为:

$$\mathrm{RMS}=\sqrt{\frac{\sum\left(\phi_s(i,j)-\phi_0(i,j)\right)^2}{N-1}} \tag{7}$$

式中，$\phi_s(i,j)$ 是滤波后的相位值，$\phi_0(i,j)$ 是参考干涉图相位值。$N$ 是滑动窗口像元个数。

(4) 相位奇异点(Residue point number)(廖明生 & 林晖, 2003)。干涉图滤波的主要目的是为了相位解缠工作的顺利进行，而相位奇异点的数量将会直接影响到解缠结果的可靠性和稳健性。因此相位奇异点的数量是衡量滤波效果的重要指标。

表 2 列出了模拟干涉相位图滤波结果的评价指标值。从表 2 可以看出：与 Lee 和 Goldstein 算法相比，新滤波算法的 PSD 和 RMS 值均最小，因此具有最好的平滑度。进一步的实验表明：本文算法的相位标准偏差(PSD)比 Goldstein 滤波器采用 0.9 的滤波因子还要略小，相位平滑效果更好。而且，新滤波算法的边缘保持指数为 1.0595，比 Lee 和 Goldstein 滤波法更接近于 1，因此具有更好的边缘保持能力。因此，新滤波算法不仅具有最好的平滑度，而且最大程度的保持了相位边缘和细节信息，具有良好的保真性和信息恢复重建能力。在相位奇异点数上，新滤波算法和 Lee 算法相当，使相位奇异点减少率达到了 99.98%，表明新滤波器在相位奇异点去除效果上的亦有良好特性。

**表 2** 模拟干涉相位图滤波结果评价指标对比

| 滤波方法 | 相位标准偏差 PSD | 边缘保持指数 EPI | 奇异点数 | 均方误差 RMS/rad |
|---|---|---|---|---|
| 原始干涉图 | 92762 | – | – | – |
| 加噪干涉图 | 324490 | 8.5053 | 16287 | 0.9142 |
| Lee 滤波 | 116380 | 1.6473 | 2 | 0.2381 |
| Goldstein 滤波 | 157520 | 3.4335 | 1313 | 0.4416 |
| 新滤波 | 101310 | 1.0595 | 4 | 0.2015 |

## 5 真实数据的验证

本文采用日本 ALOS 卫星 PALSAR 传感器河南地区 2007 年 6 月和 9 月两景相隔 90d 的 L 波段影像，其垂直基线为 282m。通过 Gamma 软件进行干涉测量数据处理，得到去除平地效应的干涉图。从得到的干涉图选取相位细节和边缘信息比较丰富 1000×1000 区域，采用本文的方法以及 Goldstein 和 Lee 滤波方法进行滤波，滤波的结果显示于图 4。

经过对比分析，可以看出新滤波方法在去除噪声的同时较好的保存了相位图的细节。尤其是在中上部条纹细节比较丰富的区域较完整的恢复了干涉相位信息，Goldstein 频域滤波结果则显得比较模糊。各种滤波方法的统计结果列于表 3。从表 3 可以看出，不论是 PSD 值还是奇异点数，新方法均优于 Lee 和 Goldstein 方法。更重要的是，由于 Lee 方法先要进行相位解缠，运用 Lee 滤波非常耗时，实验中该图滤波耗费了近 6h(表 3)。

**表 3** 真实干涉相位图滤波结果相位标准偏差残点数对比

| 滤波方法 | 相位标准偏差 PSD | 奇异点数 | 奇异点减少率/% | 运算时间/min |
|---|---|---|---|---|
| 真实干涉图 | 1507300 | 137177 | – | – |
| Lee 滤波 | 641210 | 1412 | 98.97 | 349.75 |
| Goldstein 滤波 | 972610 | 29009 | 78.85 | 1.32 |
| 新滤波 | 514330 | 939 | 99.31 | 6.18 |

## 6 结论和讨论

本文把相干性引入空域滤波中，根据相干性来选择线性方向窗口的个数，利用最优化融合的方法对所选线性方向窗口进行融合。切线方向线性窗口的频谱和噪声特性，使得选择线性方向窗口滤波有效的抑制了条纹模糊畸变效应。本方法不仅考虑了相位的局部统计信息，而且通过引入相干性实现了

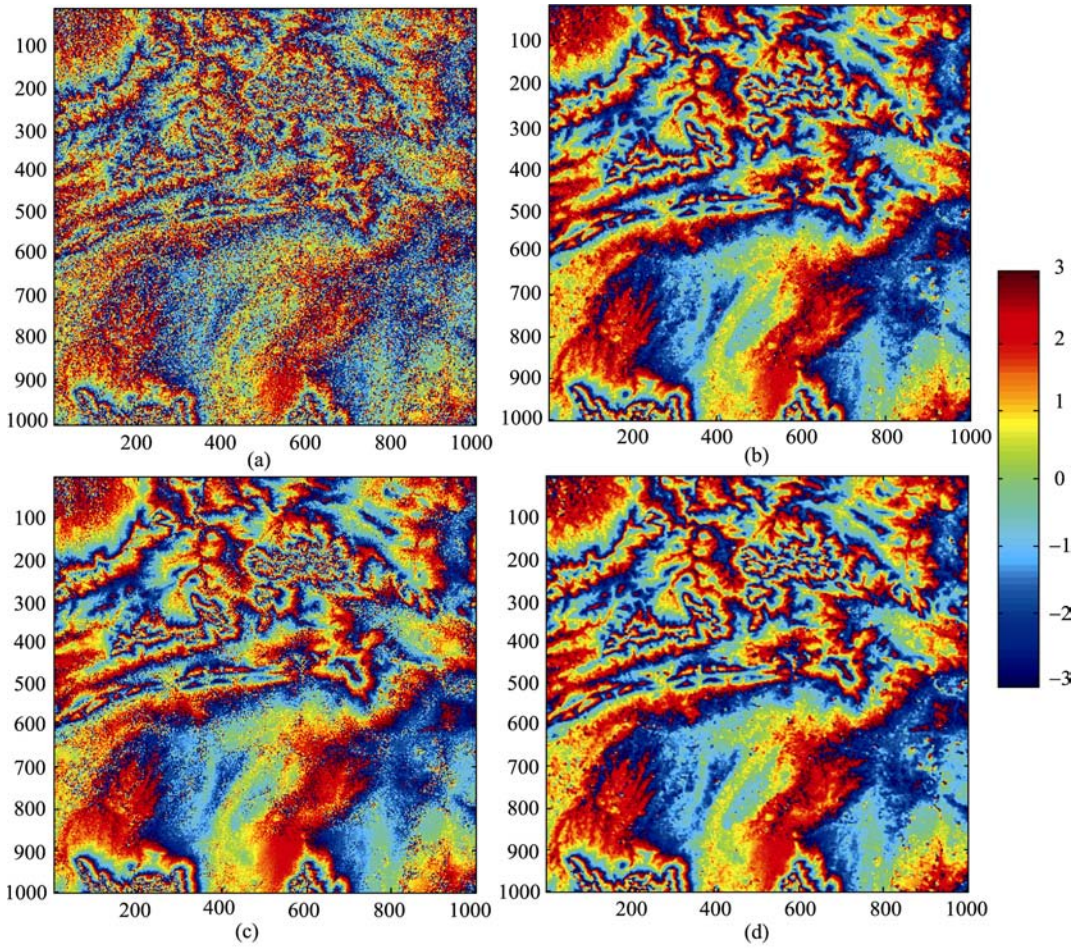


图 4 3 种滤波后的真实干涉相位图

(a) 原始干涉图; (b) Lee 滤波; (c) Goldstein 滤波; (d) 新方法滤波

自适应滤波。利用相干性作为影响因子，选择线性方向窗口的个数，在强噪区域(低相干性区域)选择较多的线性方向窗口融合，加大平滑力度；在低噪区域(高相干性区域)选择较少的线性方向窗口融合，较好的保持图像的细节，减少信息的丢失。对 L 波段的模拟和真实数据的滤波结果证实，本文提出的方法在抑制噪声的同时极大程度的减少了信息的丢失，较好的保持了干涉图的边缘和细节信息。

但是在本文的研究中发现，由于滤波本身的限制，无论采用何种滤波方法进行改善，都不可避免的会造成信息的丢失和干涉图失真。而且在强噪的情况下(相干性低于 0.1)，各种滤波方法无法得到满意的效果。当噪声在数量上大于信号时，会引起利用噪声来滤除信号。此时，无法运用滤波的方法来复原丢失的信息。

本文所提出的算法，尽管有较好的去噪和保留信息的效果，但当条纹特别密集，应用本算法无法得到满意的结果。另外该算法的复杂度也有待改善。这也是笔者下一阶段要研究的问题。

**致 谢** 感谢日本空间局提供的 ALOS 卫星 PALSAR 数据。

## REFERENCES

Baran I, Stewart M P, Kampes B M, Perski Z and Lilly P. 2003. A modification to the Goldstein radar interferogram filter. *IEEE Trans. Geosci. Remote Sensing*, **41**(9): 2114—2118

Ding X L, Liu G X, Li Z W, Li Z L and Chen Y Q. 2004. Ground subsidence monitoring in Hong Kong with satellite SAR interferometry. *Photogrammetric Engineering and Remote Sensing*, **70**(10): 1151—1156

Eichel P H and Ghiglia D C. 1993. Spotlight SAR Interferometry for Terrain Elevation Mapping and Interferometric Change Detection. Sandia National Labs. Tech. Report

Goldstein R M and Werner C L. 1998. Radar interferogram filtering for geophysical applications. *Geophy. Res. Lett.*, **25**(21): 4035—4038

Gong C L. 2007. Image smoothing method based on data fusion technology. *Journal of Jiaying University* (*Natural Science*), **25**(3): 81—84

Han C M, Guo H D, Wang C L , Fan D and Sang H Y. 2003. Edge-preserving filter for SAR images. *Chinese High Technology Letters*, **7**: 11—15

Hanssen R H. 2001. Radar Interferometry: Data Interpretation and Error Analysis. Kluwer Academic Publishers Netherlands

Lee J S, Papathanassiou K P, Ainsworth T L, Grunes M R and Reigber A. 1998. A new technique for noise filtering of SAR interferogram phase images. *IEEE Trans. Geosci. Remote Sensing*, **36**(5): 1456—1465

Li Z L, Zou W B, Ding X L, Chen Y Q and Liu G X. 2004. A quantitative measure for the quality of InSAR interferograms based on phase differences. *Photogrammetric Engineering and Remote Sensing*, **70**(10): 1131—1137

Li Z W, Ding X L, Huang C, Zhu J J and Chen Y L. 2008. Improved filtering parameter determination for the goldstein radar interferogram filter. *ISPRS Journal of Photogrammetry and Remote Sensing*, **63**: 621—634

Li Z Y, Li G D and Zhang J X. 1998. Multi-sensor data fusion and Simulation. *Journal of Jiangsu University* (*Natural Science Edition*), **19**(6): 95—100

Liao M S and Lin H. 2003. Synthetic Aperture Radar Interferometry: Principle and Signal Processing. Beijing: Mapping Press

Liao M S, Lin H , Zhang Z X, Yang W and Zhang L. 2003. Adaptive algorithm for filtering interferometric phase noise. *Journal of Remote Sensing*, **7**(2): 98—105

Massonnet D, Rossi M, Cesar C, Frederic A, Gilles P, Kurt F and Thierry R. 1993. The displacement field of the Landers earthquake mapped by radar interferometry. Nature, **364**(8): 138—142

Yu Q F, Lu H W and Liu X L. 2002. Image-based Precise Measurement and Movement Measurement. Beijing: Science Press

Zebker H A and Goldstein R M. 1986. Topographic mapping from interferometric synthetic aperture radar observations. *J. Geophy. Res.*, **91**(BS): 4993—4999

Zebker H A and Villasenor J. 1992. Decorrelation in interferometric radar echoes. *IEEE Trans. Geosci. Remote Sensing*, **30**(5): 950—959

Zisk S H. 1972. A new Earth-based radar technique for the measurement of lunar topography. *Moon*, **4**: 296—306

## 附中文参考文献

龚昌来. 2007. 基于数据融合技术的图像平滑方法. 嘉应学院学报, **25**(3): 81—84

韩春明, 郭华东, 王长林, 范典, 桑会勇. 2003. 保持边缘的SAR图像滤波方法. 高技术通讯, **7**: 11—15

李勇智, 李国栋, 张际先. 1998. 多传感器信息融合方法与仿真. 江苏理工大学学报, **19**(6): 95—100

廖明生, 林珲, 张祖勋, 杨文, 张力. 2003. INSAR 干涉条纹图的复数空间自适应滤波. 遥感学报, **7**(2): 98—105

廖明生, 林珲. 2003. 雷达干涉测量学: 原理与信号处理基础. 北京, 测绘出版社

于起峰, 陆宏伟, 刘肖琳. 2002. 基于图像的精密测量与运动测量. 北京, 科学出版社